Meyer, S.; Bennici, S.; Vaulot, C.; Rigolet, S.; Dzene, L.:
INFLUENCE OF THE PRECURSOR AND THE TEMPERATURE OF SYNTHESIS ON THE STRUCTURE OF SAPONITE.
In: Clays and Clay Minerals. Vol. 68 (2020) 544 - 552.

First published online by Clay Minerals Society: 28.10.2020

https://dx.doi.org/10.1007/s42860-020-00099-1

This is a post-peer-review, pre-copyedit version of an article published in *Clays and Clay Minerals*. The final authenticated version is available online at: http://dx.doi.org/10.1007/s42860-020-00099-1

INFLUENCE OF THE PRECURSOR AND THE TEMPERATURE OF SYNTHESIS ON THE STRUCTURE OF SAPONITE

Sebastian Meyer[1,2], Simona Bennici[1], Cyril Vaulot[1], Séverinne Rigolet[1] & Liva Dzene[1,*]

[1]Institut de Science des Matériaux de Mulhouse CNRS UMR 7361, Université de Haute-Alsace, Université de Strasbourg, 3b rue Alfred Werner, 68093 Mulhouse, Cedex, France

[2]Metallic Biomaterials, Helmholtz-Zentrum Geesthacht, Max-Planck-Str. 1, 21502 Geesthacht, Germany

ABSTRACT

Several procedures of hydrothermal synthesis of saponite can be found in the literature. They differ in terms of the preparation conditions of the precursor and of the synthesis temperature. The objective of this study was to investigate how these two parameters influence the structure of the final synthesis product. The precursor was prepared from $Mg(NO_3)_2$, $Al(NO_3)_3$ and Na_4SiO_4 in three different ways: as a gel, a dried gel and a calcined gel. The influence of the synthesis temperature on the structure of saponite was investigated in 90 – 200 °C range. The results showed that the use of calcined precursor yields a single mineral phase, saponite with up to 90% aluminum in tetrahedral configuration. In comparison, the use of gel precursor, resulted in a product with only 60% of aluminum in the tetrahedral configuration. The synthesis temperature did not have a significant effect on saponite structure. The reported synthesis method showed

the possibility to obtain saponite with superior characteristics, in terms of crystallinity, surface acidity and thermal stability compared to natural mineral, even at 90 °C and then with a higher potential for industrial applications.

Keywords: Synthesis, Minerals, Nanoclay, Saponite, precursor

INTRODUCTION

For solid state catalysts, the surface and pore characteristics play a decisive role and are investigated with many different approaches. Mesophase templating allows to synthesise amorphous silica with defined mesoporosity of up to 10 nm (Gleiter 2000). Limitations in this approach are difficulties in large-scale production and the possibility to functionalise the surface to create catalytic active sites. Zeolites are easy to synthesise, but the access to the sites positioned inside the pores, which constitutes the biggest part due to the high internal surface area, is restricted due to the presence of micropores with a dimension < 0.8 nm and therefore not reachable by larger molecules. However, a partial inhibition of crystallization using an excess of grafted organic species can lead to intracrystalline mesoporosity with increased accessibility for active sites (Xue et al. 2012). Saponite clay minerals with an important anysotropy due to their layered structure allow a better adsorption of more complex molecules onto their surface. This makes saponite clay minerals suitable for a wide range of catalytic applications for organic molecules from cracking, isomerisation (Vogels et al. 2005) and oxydation (Trujillano et al. 2009) to the Mannich reaction (Gómez-Sanz et al. 2017). In polymer composite materials saponite nanoparticles are used to give origin to novel properties not shown before by one of the components at the macro or micro scale (Nathani et al. 2004). Improvements in the mechanical properties and hindrance to diffusion were observed. The particular properties of saponites, as the high cation

exchange capacity and important specific surface area, make them also attractive for such applications as adsorbents and in wastewater treatment (Marchesi et al. 2020). Their high surface area, thermal stability, large availability and resource friendly characteristics make the use of synthetic and natural saponites increasingly attractive in research and industry (Zhou et al. 2019; Carniato et al. 2020).

Saponites are part of the smectite group and belong to the 2:1 clay minerals, which consist of layers composed of two tetrahedral silica sheets sandwiching an octahedral sheet. For synthetic saponites, the octahedral sheet can contain various divalent metals, like Mg^{2+}, Ni^{2+}, Zn^{2+}, Co^{2+}, and Fe^{2+} (Decarreau 1981; Trujillano et al. 2011). One of the requirements of the materials intended for the catalytic use, is their thermal stability. The thermal stability is found to be higher in smectites like saponites (with Mg^{2+} as the major cation in the octahedral sheet) that are stable up to 750 °C, when compared to smectites like montmorillonites (with Al^{3+} as a major cation in the octahedral sheet) with a maximum stability temperature of 480 °C (Ames and Sand 1958).

In the tetrahedral silica sheet functional ions like Al^{3+} can isomorphously substitute Si^{4+} to create active sites. Si-O-Al groups have shown strong acidic properties as a Lewis site (Aquino et al. 2004; Zhou et al. 2019). In addition, it has been suggested in the literature that the acid activity of clay minerals could be correlated to the tetrahedral surface charge density (Davidtz 1976). Thus, a product with the most of Lewis sites and with high thermal stability at the same time, could be a structure with a high amount of Al^{3+} substitution in tetrahedral sheet, i.e. having Al/Si molar ratio equal to 0.33. The possibility to synthesize saponite clay mineral with such high amount of Al^{3+} has been previously demonstrated (Suquet et al. 1977).

In general, the formation of saponites is possible under vastly different hydrothermal conditions. Moderate conditions with temperatures between 100 and 575 °C and pressures to several kbars are most promising in terms of growth rate, yield and purity (Kloprogge et al. 1999). In the 125 – 280 °C hydrothermal temperature range, a higher temperature results in an increase of the crystalline phases for ammonium saponites, shown by Fourier-transform Infrared (FTIR) spectroscopy (Kloprogge and Frost 2000). However, the chemical composition, and thus to some extent saponite crystal structure, would not be expected to significantly change by increasing the temperature. To test this hypothesis, saponite synthesis was performed from 90 to 220 °C and a detailed characterization of the chemical composition and structure of final synthesis product was performed.

While in nature the formation of smectites is determined by the availability of elements and their speciation (Christidis and Dunham 1997), in hydrothermal synthesis the most common starting materials are solid phases, such as other aluminosilicates, glasses and gels, whose composition is close to the that of the desired clay mineral (Kloprogge et al. 1999). The effect of precursor treatments on the structure of the final synthesis products is not well investigated and therefore investigated in this work.

EXPERIMENTAL

Synthesis

0.2 M solutions of magnesium nitrate ($Mg(NO_3)_2 \cdot 6H_2O$) from Sigma Aldrich (India), aluminum nitrate ($Al(NO_3)_3 \cdot 9H_2O$) from Carlo Erba (Val de Reuil, France) and sodium orthosilicate (Na_4SiO_4) from Alfa Aesar (Karlsruhe, Germany) in distilled water (18.2 MΩ·cm) were prepared. The solutions were mixed in a beaker to form a precursor that contained a Mg/Al/Si molar ratio of 1/0.33/1. The precursor was then stirred at

93 room conditions for 3 h to achieve a homogeneous suspension. For the precursor
94 experiments the suspension was put into the autoclave directly at this stage (sample
95 labeled “Gel”) followed by the hydrothermal treatment. To reduce the water content, the
96 suspension was dried in an oven at 200 °C (sample labeled “Dried gel”). For the rest of
97 the experiments the dried gel was put into a crucible and calcined at 450 °C (sample
98 labeled “Calcined gel”). At maximum temperature the holding time was 1 h after a
99 heating rate of 5 °C/min and a cooling time of less than 10 °C/min afterwards.

100 For the hydrothermal synthesis a 0.01 M NaOH solution was prepared using NaOH
101 powder from Sigma Aldrich (St Louis, USA) and then added to the grinded calcined
102 precursor gel. The autoclave with the suspension was securely closed and placed into an
103 oven for 120 hours. The synthesis was conducted at 90, 120, 150, 180 and 200 °C. In
104 the autoclave a pressure corresponded to a water pressure at those temperatures. The pH
105 was measured with Hi2211 pH ORP Meter by Hanna Instruments (Tanneries, France)
106 with two point calibration at pH = 7 and pH = 10 after the precipitation of the precursor
107 and after the synthesis.

108 After the synthesis, samples were recovered by centrifugation at 8000 rpm for
109 10 min, which was followed by washing with distilled water two times and ion
110 exchange with Ca^{2+} using 1 M $CaCl_2$ solution (Carrado et al. 2006). The choice to
111 saturate the samples with Ca^{2+}, was driven by a practical conveniency. As Ca^{2+}-
112 saturated smectites have two water layer hydrate structure over a large relative humidity
113 range (Suquet et al. 1975), such material is then less sensitive to relative humidity
114 changes and more practical to handle during the different characterization experiments.
115 After the ion-exchange and washing, the suspension was dried in an oven at 60 °C and
116 ground in a mortar.

X-ray diffraction of powder and oriented preparations

The ground saponite powder was placed into a backloading sample holder and compacted. The prepared sample was measured by X'Pert Pro from PANalytical (Malvern, United Kingdom) equipped with an X'Celerator real-time multiple strip detector operating with an angular aperture of 2.12°2θ in 3° to 70°2θ range using CuKα radiation with the wavelength of 0.15406 nm. Diffractogrammes were recorded at room temperature with step size of 0.017°2θ and scan time of 4 s per step. The divergence slit, the anti-scatter slit and the two Soller slits were 0.0625°, 0.125°and 2.3°, respectively.

The oriented slides were prepared by placing a droplet of the diluted suspension on a glass slide to evaporate with time. Particles settled by gravity and adopted a preferable orientation parallel to the substrate. For optimal measurement results 3 to 20 mg of powder were used. The dried slides were then recorded in 3° to 35°2θ range with the same scanning parameters as before. To saturate the samples with ethylene glycol, the glass slides were put into a desiccator with ethylene glycol for 2 days.

Fourier-transform infrared spectroscopy

The synthezised saponite was mixed with potassium bromide in the weight ratio 1:100 and ground with a mortar by hand. The powder was given into a mold and pressed isostatically at 5 bar for 3 minutes. The resulting pellets were put into an oven at 150 °C overnight to reduce the water content. FTIR spectroscopy measurements were conducted with the device Equinox 55 from Bruker (Karlsruhe, Germany). The obtained spectrum was the average of 32 measurements with a resolution of 4 cm^{-1}. The software OPUS was used to record the spectra and to subtract the reference with CO_2 and H_2O contributions.

Nuclear magnetic resonance spectroscopy

The ^{27}Al MAS NMR spectra were recorded at room temperature with a Bruker Avance II 400 MHz spectrometer (Wissembourg, France) operating at B_0 = 9.4 Tesla giving a ^{27}Al Larmor frequency of 104.23 MHz, equipped with a Bruker 4 mm double channels probe. All experiments were performed at room temperature in ZrO_2 rotors, with a $\pi/12$ radio frequency pulse length of 0.5 μs, a recycle delay of 1 s, at a spinning rate of 12 kHz. The chemical shifts were referred to external $[Al(H_2O)_6]^{3+}$ in $AlCl_3$ aqueous solution. The decompositions of the spectra were performed using the DMFit software (Massiot et al. 2002).

X-ray fluorescence spectroscopy

The sample pellet was prepared by applying an isostatic pressure of 5 bar on 200 mg of sample. The spectrometer Zetium from PANalytical (Malvern, United Kingdom) was used to record the spectra that were analysed towards the composition of oxides in weight percent. The atomic weight percent was then calculated.

Nitrogen adsorption

A Micromerics ASAP 2420 (Verneuil en Halatte, France) was used to adsorb nitrogen at the temperature of liquid nitrogen (-196 °C). Prior to adsorption, 100 to 200 mg of the sample were outgassed in vacuum at 120 °C to remove the water adsorbed on the surface of the particles. The sample mass after pretreatment was measured, then the sample flask was connected to the device to be cooled down to -196 °C during the whole measurement. Specific surface area of the sample was derived with the BET method using the software MicroActive version 1.01. The average mesopore size was derived from the adsorption branch of the isotherm using the

Barrett–Joyner–Halenda (BJH) method. The micro and mesopore size distribution was derived using the density function theory (DFT). Slit and cylinder shape for oxide surfaces were tested and evaluated by their RMS (Root mean square) error of the isotherm fit and by the correct fit between the experimental isotherm and the different modelizations (step-like fits were avoided and the fits were tested in log and linear scales).

Transmission electron microscopy

Samples were prepared by dispersing the synthesized saponite powder with ultrasound in chloroform. The resulting suspension was evaporated on a carbon coated copper grid at room temperature leaving homogeneously distributed particles. The device ARM200F from JEOL (Tokyo, Japan) with an acceleration voltage of 200 kV was used to record the images. The software Digital Micrograph allowed to measure the average basal spacing by calculating the mean over 6 to 10 clay mineral layers in a selected area.

RESULTS AND DISCUSSION

Influence of precursor preparation on structure formation

The pH was 12.7 after 3 hours of the gel aging and 12.5 after the hydrothermal synthesis. The X-ray powder diffractograms (Fig. 1) of synthesis products using different precursors revealed that typical 2:1 tri-octahedral clay mineral planes (020), (200), (150) and (060) could be identified in all three samples. The basal reflection (001) at 5.9°2θ was only well-defined and symmetrical for the sample prepared from the calcined gel. It indicated an ordered structure with layer-to-layer distances of around 1.5 nm.

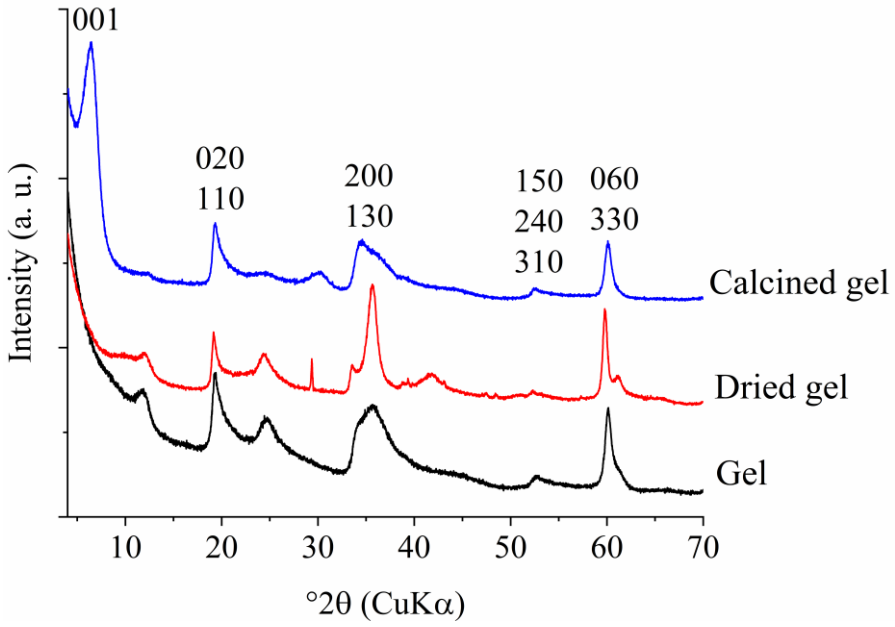

187

188 **Fig. 1** Powder XRD patterns after hydrothermal synthesis at 200 °C using different

189 precursors.

190 For the samples prepared from gel and dried gel precursors, XRD peaks at 12°

191 (0.75 nm) and 24°2θ (0.36 nm) were observed that corresponded to heterogeneous

192 formations of polymorphs of the kaolinite-serpentine group and chlorites. The peak at

193 35.7°2θ (2.51 nm) and the two peaks at 59.8°2θ (0.154 nm) and 61.1°2θ (0.151 nm)

194 suggested the presence of lizardite-like structure. Other phases like chlorites could

195 contribute to a higher amount of octahedral Al, especially for the sample prepared from

196 dried gel precursor. The XRD patterns showed crystalline and single clay mineral

197 saponite formation using the precursor of calcined gel. The product after hydrothermal

198 synthesis then contained a higher purity crystalline saponite. No characteristic peaks of

199 other aluminum phases such as alumina, gibbsite or boehmite, neither hydrotalcite-like

200 phases were identified in X-ray diffractograms. The small sharp peak at 29.5°2θ

201 (0.303 nm) corresponded to calcite, an impurity arising from an incomplete washing

202 prior to the sample saturation with Ca^{2+}.

FTIR spectroscopy was used to compare the results from XRD, regarding the sample cristallinity, and to obtain the information on the presence of amorphous aggregates and the type of bonds present in the samples. For all three samples, O-H and Si-O vibration modes, characteristic of clay minerals, could be identified (Fig. 2) (Petit 2006). The large band at ~3400 cm^{-1} and at 1629 cm^{-1} corresponded to the vibration modes of H_2O molecules. The band at 1427 cm^{-1} corresponded to carbonates, an impurity identified also by XRD. The O-H bending mode identified at 651 cm^{-1} was characteristic for tri-octahedral clay minerals (Russell and Fraser 1994).

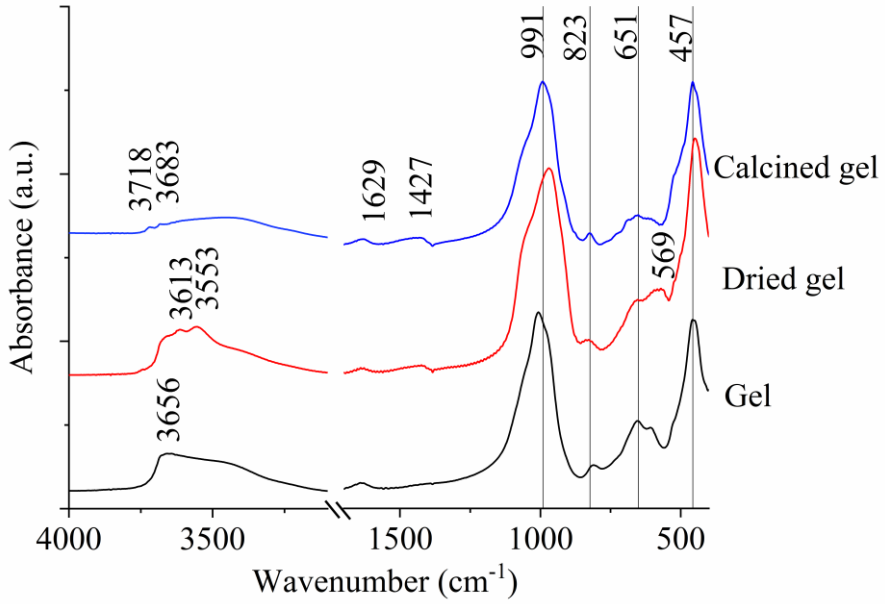

Fig. 2 FTIR spectra of saponite obtained after hydrothermal synthesis at 200 °C using different precursors.

The region of O-H stretching vibration mode was rather broad for samples prepared from the gel and dried gel precursors. Two bands of 3718 and 3683 cm^{-1} could be clearly identified for the sample prepared from calcined precursor. The bands corresponded to Mg_3O-H stretching mode. It was shown by Pelletier et al. (2003) that the bands corresponding to the hydroxyl groups were influenced by the saponite layer

charge. The Mg_3O-H peak shifted from 3676 to 3692 cm^{-1} due to bond stretching with increasing tetrahedral Al^{3+} substitutions and the compensating cation. The peak visible at 3683 cm^{-1} and additionally at 3716 cm^{-1} in our reorded spectra was then an additional evidence for Al^{3+} substitutions in the tetrahedral sheet. For the sample prepared from the gel precursor a band at 3656 cm^{-1} could be identified corresponding to Mg_2AlO-H stretching mode (Petit et al. 2004). It indicated an important substitution of Al^{3+} for Mg^{2+} in the octahedral sheet. Among the broad zone of O-H stretching mode, two bands could be distinguished for the sample prepared from the dried gel precursor: 3613 and 3553 cm^{-1}. These bands were charateristic of Al_2O-H stretching modes. In particular, 3553 cm^{-1} band was characteristic of chlorites, which was in agreement with phases identified in XRD pattern (Russell and Fraser 1994).

In all three samples, bands at 991 and 457 cm^{-1} could be clearly identified corresponding to Si-O vibration modes. In addition, a band at 692 cm^{-1} could be identified for the calcined gel sample corresponding to Si-O vibration mode as well. The substitution of Al^{3+}-for-Si^{4+} in the tetrahedral sheet is known to shift Si-O stretching mode band value from 1000 cm^{-1} towards lower values, which corresponds to the present case (991 cm^{-1}). Klopproge and Frost (2000) had attributed 457 cm^{-1} to the Si-O bending mode of amorphous silica. In the present case, as no other Si-O modes in this region could be clearly identified and considering XRD results, this could then correspond to Si-O vibration mode belonging to clay minerals. However, the presence of amorphous silica cannot be discarded. Indeed, a band ~569 cm^{-1} could be identified for the samples prepared from the gel and dried gel precursors, reported as belonging to amorphous SiO_2. Finally, all samples contain a band at 823 cm^{-1} attributed to Al-O_4

band vibration, affirming the presence of tetrahedral aluminum. The characteristic bands of alumina were not identified.

The NMR results (Fig. 3) revealed the aluminum resonances for the tetrahedral (^{IV}Al) and octahedral (^{VI}Al) configuration of all precursor types after synthesis. Signals observed around 60 and 8 ppm were attributed to ^{IV}Al and ^{VI}Al respectively. Using the gel precursor, the Al content was nearly evenly distributed between the octahedral and the two tetrahedral sheets in the final product with ^{IV}Al = 55%. The NMR spectroscopy results were in agreement with the FTIR spectroscopy results, where Mg_2AlO-H stretching mode was identified suggesting an important substitution of Al^{3+} for Mg^{2+} in the octahedral sheet. Using the dried and calcinated gel precursors the content of tetrahedral aluminum increased with ^{IV}Al = 80% and ^{IV}Al = 85%, respectively. NMR results showed a higher amount of octahedral Al in the samples prepared from the gel and dried gel precursors. In agreement with XRD results, the structure with maximum Al in the tetrahedral position was obtained using the calcined gel as precursor.

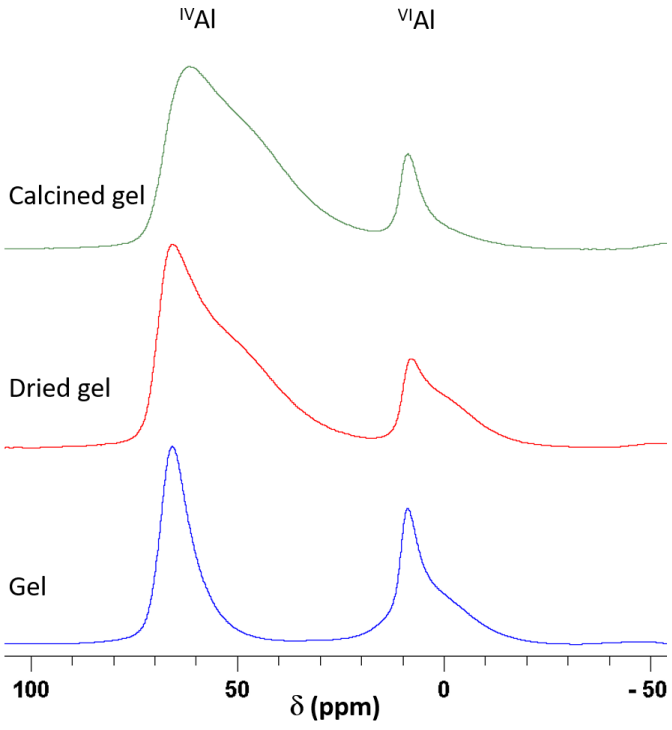

Fig. 3 ^{27}Al MAS NMR spectra of samples synthesized at 200 °C with different precursor preparation methods. ^{VI}Al and ^{IV}Al corresponds to the chemical shift (δ) of octahedrally and tetrahedrally coordinated aluminum respectively.

In summary, three different characterization techniques: XRD, FTIR and NMR spectroscopies, indicated that the sample prepared from calcined gel precursor gave better defined structure of saponite with a maximum substitution in the tetrahedral sheet compared to samples prepared with the gel and dried gel precursors. The initial precipitation of precursor was expected to create a homogenous gel from its constituents (Hamilton and Henderson 1968). The calcination of precursor removed water, and it was then expected that more amorphous regions with a large number of defects were created. Moreover, amorphous and crystalline $Al(OH)_3$ containing compounds could undergo phase transitions at temperatures between 130 and 450 °C and were more likely to disappear during the calcination of the precursor (Walker 1993; Földvári 2011). Also, during drying, water was gradually evaporated and a very basic environment could be locally created thus favoring the formation of tetrahedral Al^{3+}. The obtained powder from calcined precursor was amorphous and very reactive upon dissolution and subsequent forming of crystalline phase in hydrothermal synthesis experiments.

Influence of synthesis temperature on structure formation

The increase of temperature could be expected to enhance the sample crystallinity, as shown by Kloprogge and Frost (2000). The calcined gel precursor was used to synthesize saponites at five different temperatures from 90 to 200 °C. The powder XRD pattern (Fig. 4) showed the regular saponite structure nearly independent from the synthesis temperature, without crystalline secondary phases. The layer-to-layer distances were between 1.43 and 1.48 nm with a slight trend to increase with synthesis

temperature. Such layer-to-layer distance corresponds to Ca^{2+}-saturated saponite with two layers of the water in the interlayer (Suquet et al. 1977).

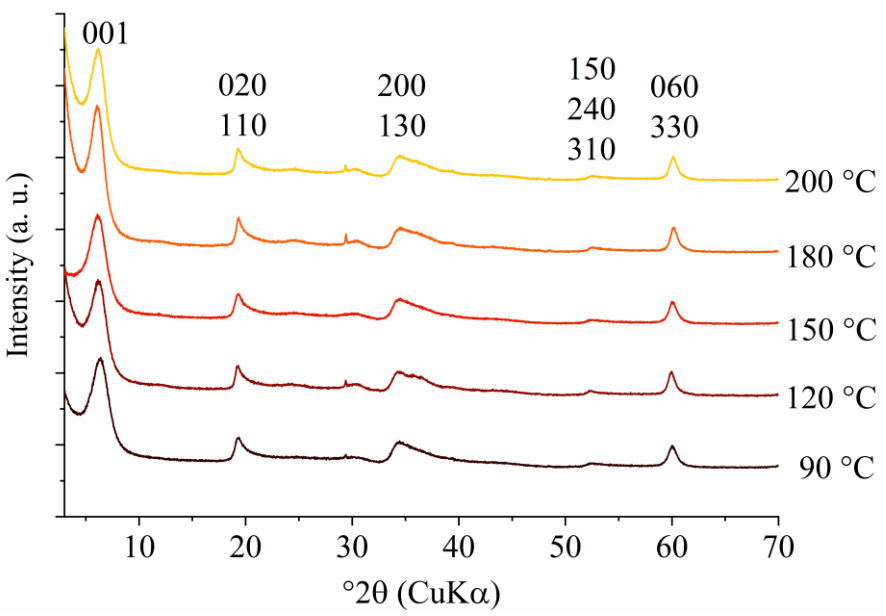

Fig. 4 Powder XRD pattern of synthetic saponite with indexed diffraction planes at different temperatures. d_{001}=1.5 nm and d_{060}= 0.154 nm.

The swelling property (typical of smectite clay minerals) was assessed using the saturation of oriented preparations with ethylene glycol (Fig. 5). For such preparations, the 001 reflection was pronounced because of the alignment of particles, and shifted its position when saturated with ethylene glycol due to the increase of the layer-to-layer distance. Only a slight shift of around 0.05 to 0.1 nm was observable and indicated a high charge of the layers as expected. Substitution of Al^{3+}-for-Si^{4+} in the silicate sheets resulted in a more localized charge that had to be compensated by interlayer cations compared to the aluminum substitution in the octahedral sheet, which was compensated over a larger volume by slightly more negatively charged oxygen atoms (Kloprogge et al. 1999). The analysis of oriented slides indicated smaller layer-to-layer distances for the lower synthesis temperatures (90 and 120 °C) suggesting a stronger interaction

between the layers and more pronounced localization of the charge in the tetrahedral sheets. Moreover, the diffraction peak was broadened with the decrease of the temperature, suggesting a smaller particle size and/or more heterogeneous structure.

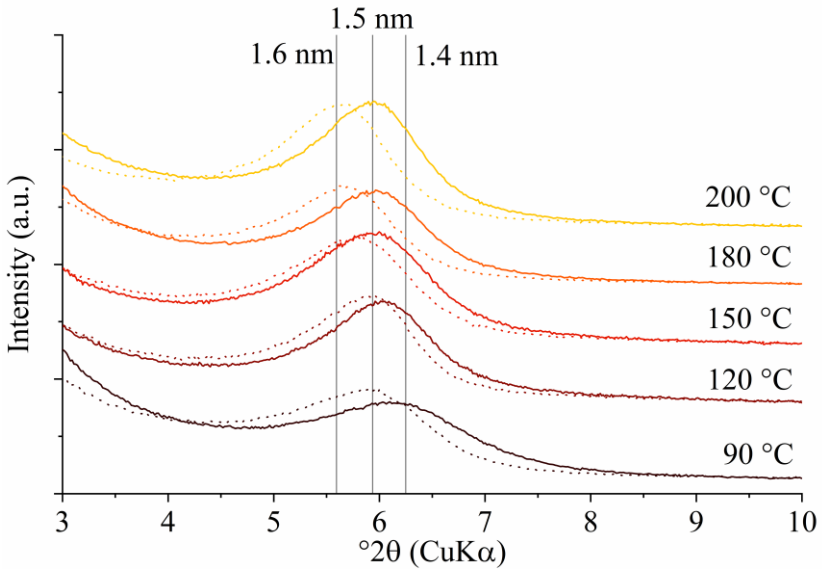

Fig. 5 XRD patterns of 001 reflection of oriented slides at ambient conditions (solid line) and after ethylene glycol saturation (dotted line) with d_{001} indicated above.

For a better insight into the amorphous phases and their bond structure, FTIR spectra were acquired for sample prepared at each synthesis temperature. The identified bands corresponded to bonds in saponite structure, as previously discussed in section 3.1 (Fig.6). The peak shapes at 991 and 457 cm^{-1} corresponding to Si-O vibration modes expressed a higher crystallinity for the synthesis at 200 °C. At lower synthesis temperatures the reduced and broader peaks indicated smaller particle size and/or more heterogenous structures. Apart from the Si-O vibration bands, the rest of the spectrum seemed nearly unaffected by the synthesis temperature.

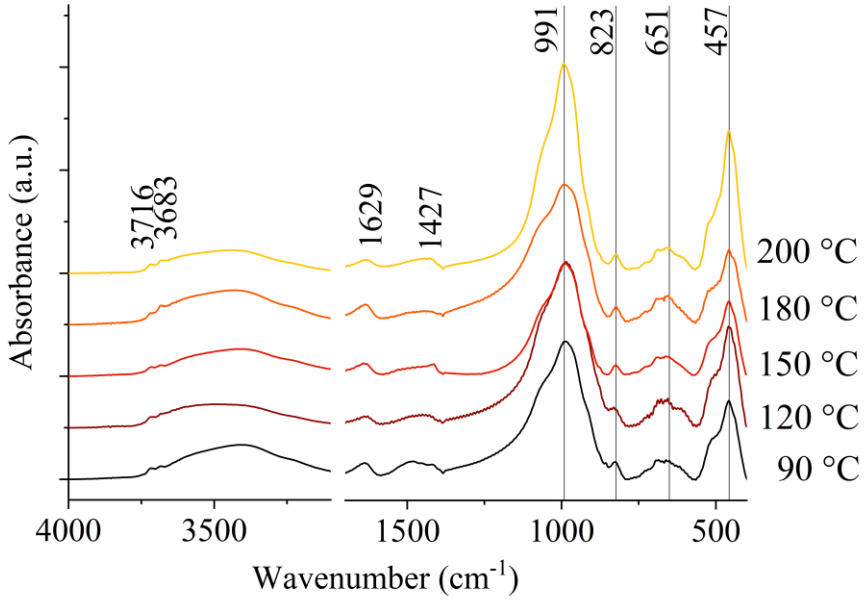

Fig. 6 FTIR spectra of saponite synthesized at different temperatures.

To obtain structural information about the location of aluminum in the structure, NMR spectroscopy measurements were performed (Fig. 7). With the synthesis procedure used, the aluminum content in the tetrahedral sheet was about 80 to 90%, while the octahedral sheet only contained the small remaining amount. There was a slight trend towards a higher amount of octahedral Al at high synthesis temperatures (Table 1). This result was in agreement with the trend observed by the XRD experiment

performed on oriented slides, which suggested the localization of the charge in the tetrahedral sheet with the decrease of the synthesis temperature. But because the quantification of the NMR data is rather approximate and a deviation of 5 to 10% should be assumed for interpretation, this trend had to be handled with care. Nevertheless, it can be stated that even at low synthesis temperatures the vast majority of the substitution by Al happened in the tetrahedral sheet.

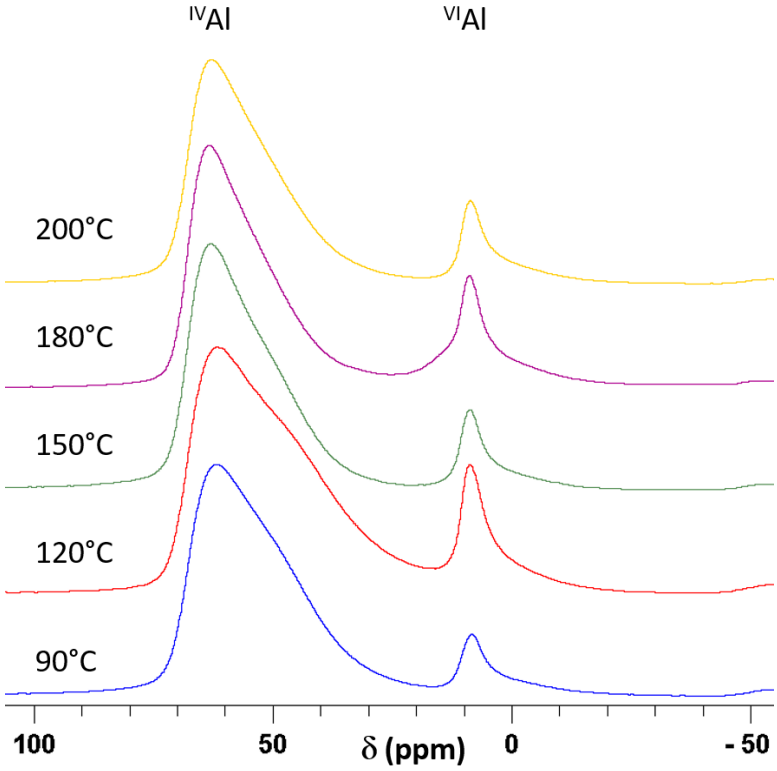

Fig. 7 ^{27}Al MAS NMR spectra of saponite synthesized at different temperatures indicating aluminum in octahedral (^{VI}Al) and tetrahedral sheet (^{IV}Al).

The chemical composition of synthesized products was analyzed by XRF spectroscopy. The highest Al/Si and Ca/Si molar ratios were obtained for samples synthesized at 90 and 120 °C (Table 1). The higher amount of interlayer Ca^{2+} correlated with the increased amount of Al substitutions in the structure. Assuming that no other phases were present in significant amounts, and that probably a slightly higher amount

of Al was located in the tetrahedral sheets compared to octahedral sheets for samples prepared at a lower synthesis temperature, these results could then also be correlated to the XRD experiments on oriented slides. The analysis of oriented slides lead to the hypothesis that for the lowest synthesis temperatures (90 and 120 °C) the charge was mainly localized in the tetrahedral sheets. These results were then in good agreement with the chemical composition and NMR results.

Table 1. Element molar ratios obtained by XRF and calculated ratio of tetrahedral aluminum obtained by NMR spectroscopy. Surface area and average pore size calculated from N_2 adsorption measurement.

Synthesis temperature	Al/Si molar ratio	Mg/Si molar ratio	Ca/Si molar ratio	^{IV}Al by NMR (%)	S_{BET} (m^2/g)	Average pore size (nm)
90 °C	0.42	1.13	0.21	90	172	6.0
120 °C	0.41	0.96	0.20	85	131	8.7
150 °C	0.35	0.99	0.17	90	173	6.2
180 °C	0.36	1.01	0.16	80	113	7.0
200 °C	0.35	0.98	0.17	80	179	6.7

The creation of functional groups, as the Lewis acid groups, requires a maximum tetrahedral substitution. Here, the sample synthesized at 90 °C, using calcined precursors, showed that a high amount of functional groups could be created even at low temperature. In comparison with the study of Kloprogge and Frost (2000), where a shorter synthesis time (3 days instead of 5 days) and a temperature of 280 °C were used, well defined saponite structure could be obtained even at lower temperature.

Nanostructure and porosity

Although the synthesis at 90 °C seemed to be the most promising, the FTIR spectroscopy results suggested a higher homogeneity and/or better crystallinity for the

sample synthesized at 200 °C. Thus, with XRD and FTIR spectroscopy results alone, it remained unclear how amorphous constituents might be distributed. The observations of samples synthesized at three different temperatures (90, 150 and 200 °C) under TEM were undertaken to obtain an overview of particle size and shape (Fig. 8). The particle size was visually estimated to be between 50 and 100 nm. The TEM images showed a majority of crystalline regions, which was in agreement with the XRD and FTIR spectroscopy results. No particular difference, in terms of particle size and presence of amorphous aggregates, was observed among the samples synthesized at different temperatures. Thus, the slight differences observed by the XRD and FTIR spectroscopy analysis of oriented slides among the various samples could be due to the inhomogeneity of structure in terms of Al distribution in the structure, which increased with decreasing the temperature. In the TEM pictures the layer fringe contrast was used to approximate the basal spacing. In all locations chosen, the values were found between 0.9 to 1.1 nm. This was considerably smaller than the 1.4 to 1.5 nm obtained by powder XRD. This was due to the removal of interlayer water in the ultra-high vacuum. It has to be noted that the estimation of basal spacing was only approximate due to the unknown exact orientation angle of the layers.

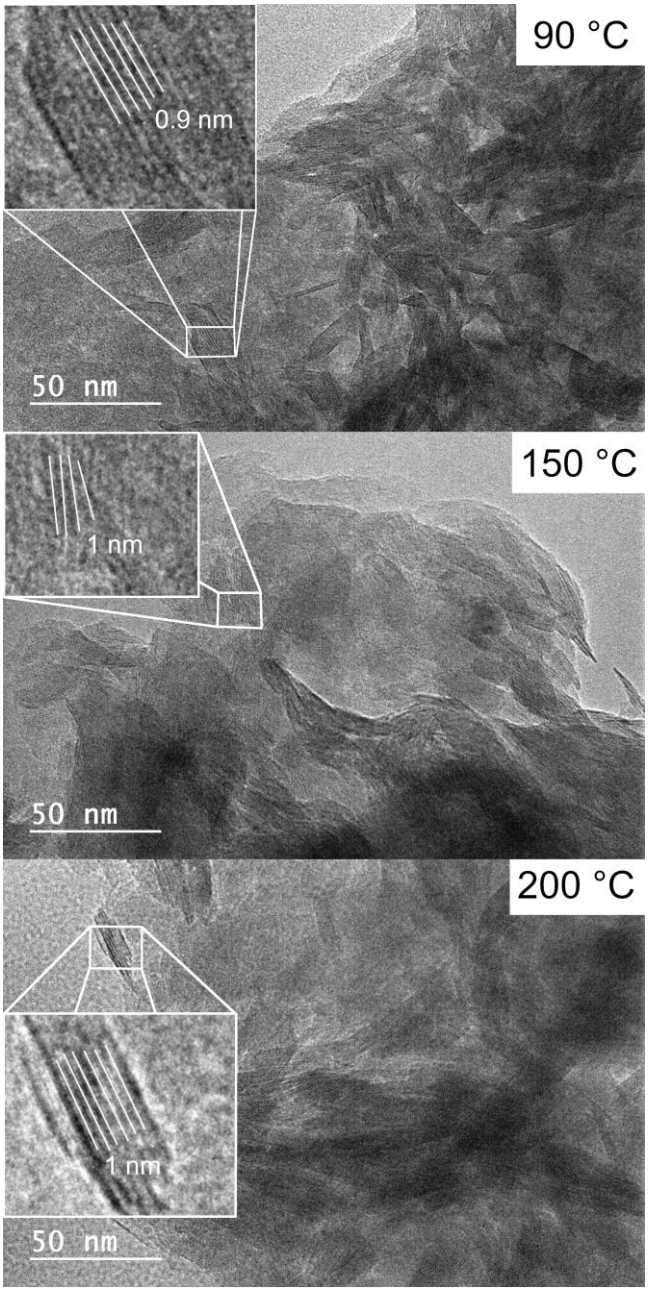

Fig. 8 TEM images of saponite synthesized at different temperatures. Basal spacings derived by lattice fringe contrast.

N_2 adsorption measurements (Fig. 9) provided additional insight about the microstructure of the samples giving information about the accessible surface area, pore volume, and pore size distribution and shape. Adsorption at low relative pressure corresponded to the filling of the microporosity and at higher pressure to the

mesoporosity. The specific surface area for each synthesis temperature, determined by the BET method, was up to 179 m^2/g (Table 1). The samples prepared at 120 and 180 °C presented the lowest specific surface area. This did not correlate to the microstructural features investigated earlier and might therefore be connected to the sample preparation previous to the isotherm acquisition. The analysis of the shape of the isotherms (and of the hysteresis) gave information about the pore shape. The adsorption curve was a type IV and hysteresis was of H2 type, according to IUPAC classification. The hysteresis shape corresponded to ink bottle shape cavities, which needed to reach a critical pressure (quite lower than during adsorption) in order to desorb nitrogen. Applying the BJH method, average pore sizes of 6 to 8.7 nm was obtained (Table 1).

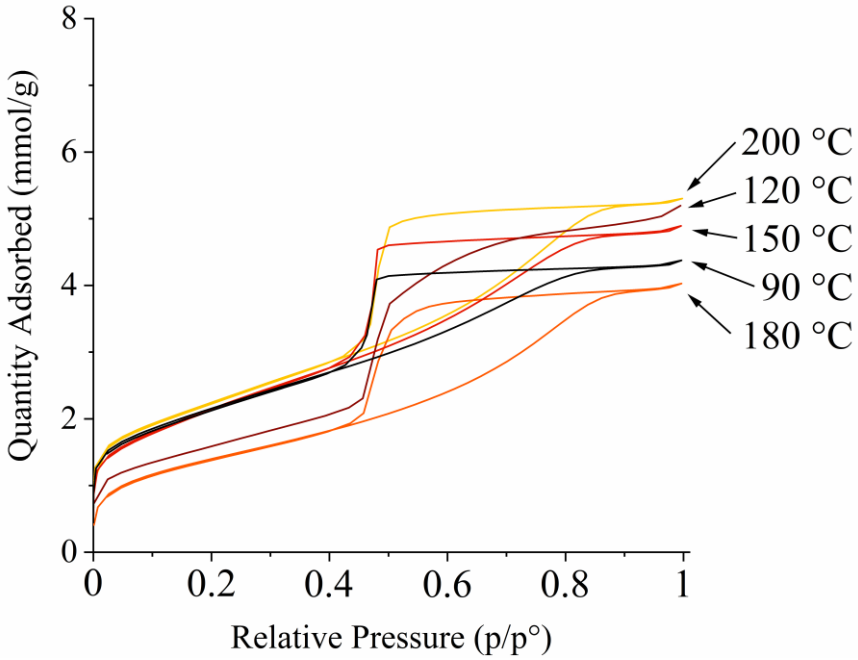

Fig. 9 Isotherms of nitrogen adsorption and desorption for saponites synthesized at different temperatures.

With the t-plot technique, a small amount of micropores could be identified. Occelli et al. (2002) found micropores with the diameter of 1.5 nm using the DFT model. The derivative of the pore volume over the pore width calculated by the DFT model was

then also applied in this study. Clay minerals are known for their layered structure, which means that a slit-like pore shape with constant height but larger and varying width and length could be expected. However, the overall RMS error of the isotherm fit was significantly lower assuming a cylindrical pore shape than a slit one. The distribution showed two pore domains (Fig. 10).

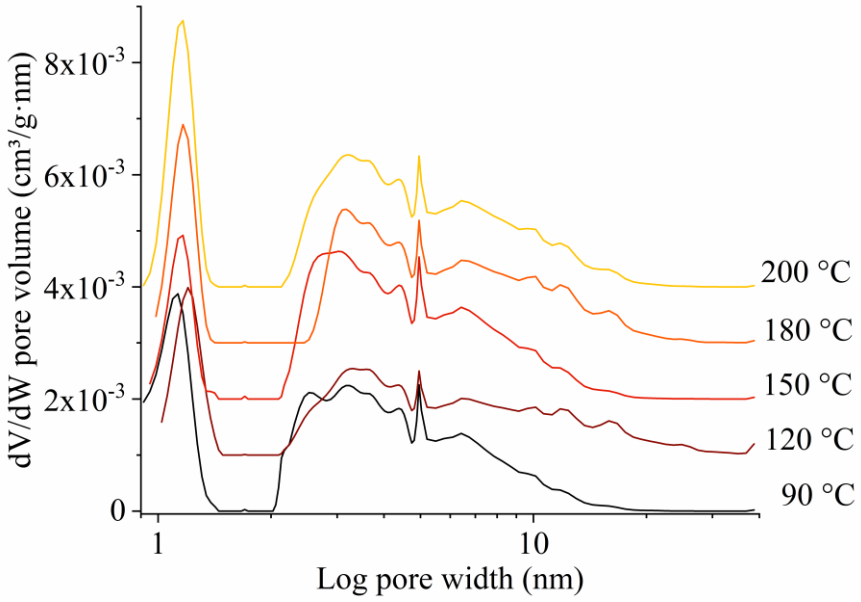

Fig. 10 Pore size distribution derived from the adsorption isotherm with the DFT method assuming cylindrical pores on oxide surface with regularization of 0.1 .

The micropores were narrowly distributed around 1.1 nm. For the samples obtained at 120 and 180 °C nearly no micropores could be found by DFT. No clear trend in the pore size was observable for increasing synthesis temperature. Instead, the pore distribution seemed to remain the same. The mesoporous domain above 2 nm was at the origin of the most part of the pore volume. On the other hand, micropores contributed to the increase of surface area and their absence in these two samples explained the lower BET specific surface area measured. If existing, pillars in between the layers could result in more cylindrical shapes, but such structures were not revealed by XRD, FTIR spectroscopy or TEM, and they could be then excluded. However, applying a

409 cylindrical pore shape a better fit with the presence of mesopores could be obtained,
410 which contributed largely to the total volume. These observations showed the
411 discrepancy on the application of the various models, since it is not easy to differentiate
412 among different pore shapes for a certain pore dimension. Cylindrical mesopores could
413 be more likely created in the intercrystallite spaces formed during aggregation.
414 Therefore, the pore size distribution and shape did not correlate (or only partially) to the
415 materials intrinsic properties, as the charge, but to the preparation unitary steps, as
416 grinding, sieving and outgassing.

417 ## CONCLUSIONS

418 In this study, saponites were synthesized and the influence of the heat treatment of
419 the precursor was shown. The characterization of the synthesized products by XRD and
420 FTIR spectroscopy indicated that a homogenous powder of saponite (in terms of
421 structure and chemical composition) could be obtained using a precursor calcined at
422 450 °C. Additionally, a higher quantity of aluminum in tetrahedral configuration was
423 measured for this sample, which might bring to a higher thermal stability and a higher
424 amount of acidic groups useful in catalysis. By using the calcined precursor,
425 hydrothermal synthesis performed at low temperature (90 °C) allowed to obtain a high
426 purity saponite. A synthesis temperature of 200 °C resulted in a very similar product,
427 probably presenting a slightly improved homogeneity, but with lower layer charge and
428 consequently less tetrahedral aluminum.

429 The distribution of mesopores was found to be in the 2 to 11 nm range, promising for
430 the accessibility of large organic molecules. Additionally, it was shown that pillaring or
431 acidic activation could further increase the accessible surface area (Kloprogge 1998;
432 Michot et al. 1998; Trombetta et al. 2000). In contrast to montmorillonite, saponite can

433 be more easily modified by acidic leaching due to of the presence of octahedral
434 magnesium. Such acidic treatments could greatly enhance the microporosity and
435 specific surface area (up to 510 m^2/g) (Vicente et al. 1996; Bisio et al. 2008).

436 ## ACKNOWLEDGEMENTS

437 N_2 adsorption experiments, XRD, XRF, NMR and TEM analysis were performed on
438 the technical plateforms of IS2M. The authors are grateful to Laure Michelin, Loïc
439 Vidal and Habiba Nouali for their contribution. The internship of Sebastian Meyer was
440 funded by IS2M/UHA in the frame of an "Emerging" project call.

441

442 On behalf of all authors, the corresponding author states that there is no conflict of
443 interest.

444 ## REFERENCES

445 Ames, L.L. & Sand, L.B. (1958) Factors effecting maximum hydrothermal stability in
446 montmorillonites. *The American Mineralogist*, *43*, 641–648.
447 Aquino, A.J.A., Tunega, D., Gerzabek, M.H., & Lischka, H. (2004) Modeling catalytic
448 effects of clay mineral surfaces on peptide bond formation. *Journal of Physical*
449 *Chemistry B*, *108*, 10120–10130.
450 Bisio, C., Gatti, G., Boccaleri, E., Marchese, L., Bertinetti, L., & Coluccia, S. (2008) On
451 the acidity of saponite materials: A combined HRTEM, FTIR, and solid-state
452 NMR study. *Langmuir*, *24*, 2808–2819.
453 Carniato, F., Gatti, G., & Bisio, C. (2020) An overview of the recent synthesis and
454 functionalization methods of saponite clay. *New Journal of Chemistry*, *44*, 9969–
455 9980.

456 Carrado, K.A., Decarreau, A., Petit, S., Bergaya, F., & Lagaly, G. (2006) Synthetic Clay
457 Minerals and Purification of Natural Clays. In F. Bergaya, B.K.G. Theng, & G.
458 Lagaly (Ed.), Handbook of Clay Science. (pp. 115–139). Elsevier.
459 Christidis, G. & Dunham, A.C. (1997) Compositional variations in smectites. Part II:
460 alteration of acidic precursors, a case study from Milos Island, Greece. *Clay*
461 *Minerals*, *32*, 253–270.
462 Davidtz, J.C. (1976) The acid activity of 2:1 layer silicates. *Journal of Catalysis*, *43*,
463 260–263.
464 Decarreau, A. (1981) Cristallogenese à basse température de smectites trioctaèdriques
465 par vieillissement de coprécipités silicométalliques. *Comptes rendus des séances*
466 *de l'Académie des sciences*, *292*, 61–64.
467 Földvári, M. (2011) *Handbook of Thermogravimetric System of Minerals and Its Use in*
468 *Geological Practice*. Geological Institute of Hungary, Budapest.
469 Gleiter, H. (2000) Nanostructured materials: basic concepts and microstructure. *Acta*
470 *Materialia*, *48*, 1–29.
471 Gómez-Sanz, F., Morales-Vargas, M.V., González-Rodríguez, B., Rojas-Cervantes,
472 M.L., & Pérez-Mayoral, E. (2017) Acid clay minerals as eco-friendly and cheap
473 catalysts for the synthesis of β-amino ketones by Mannich reaction. *Applied Clay*
474 *Science*, *143*, 250–257. Elsevier.
475 Hamilton, D.L. & Henderson, C.M.B. (1968) The preparation of silicate compositions
476 by a gelling method. *Mineralogical Magazine*, *36*, 832–838.
477 Kloprogge, J.T. (1998) Synthesis of smectites and porous pillared clay catalysts: a
478 review. *Journal of Porous Materials*, *5*, 5–41.
479 Kloprogge, J.T. & Frost, R.L. (2000) The effect of synthesis temperature on the FT-

480 Raman and FT-IR spectra of saponites. *Vibrational Spectroscopy*, *23*, 119–127.
481 Kloprogge, J.T., Komarneni, S., & Amonette, J.E. (1999) Synthesis of smectite clay
482 minerals: A critical review. *Clays and Clay Minerals*, *47*, 529–554.
483 Marchesi, S., Carniato, F., Guidotti, M., Botta, M., Marchese, L., & Bisio, C. (2020)
484 Synthetic saponite clays as promising solids for lanthanide ion recovery. *New*
485 *Journal of Chemistry*, *44*, 10033–10041.
486 Massiot, D., Fayon, F., Capron, M., King, I., Le Calvé, S., Alonso, B., Durand, J.-O.,
487 Bujoli, B., Gan, Z., & Hoatson, G. (2002) Modelling one- and two-dimensional
488 solid-state NMR spectra. *Magnetic Resonance in Chemistry*, *40*, 70–76.
489 Michot, L.J., Villiéras, F., Lambert, J.F., Bergaoui, L., Grillet, Y., & Robert, J.L. (1998)
490 Surface heterogeneity in micropores of pillared clays: The limits of classical pore-
491 filling mechanisms. *Journal of Physical Chemistry B*, *102*, 3466–3476.
492 Nathani, H., Dasari, A., & Misra, R.D.K. (2004) On the reduced susceptibility to stress
493 whitening behavior of melt intercalated polybutene-clay nanocomposites during
494 tensile straining. *Acta Materialia*, *52*, 3217–3227.
495 Occelli, M.L., Olivier, J.P., Peridon-Melon, J.A., & Auroux, A. (2002) Surface area,
496 pore volume distribution, and acidity in mesoporous expanded clay catalysts from
497 hybrid density functional theory (DFT) and adsorption microcalorimetry methods.
498 *Langmuir*, *18*, 9816–9823.
499 Pelletier, M., Michot, L.J., Humbert, B., Barrès, O., D'Espinose de la Caillerie, J.B., &
500 Robert, J.L. (2003) Influence of layer charge on the hydroxyl stretching of
501 trioctahedral clay minerals: A vibrational study of synthetic Na- and K-saponites.
502 *American Mineralogist*, *88*, 1801–1808.
503 Petit, S. (2006) Fourier Transform Infrared Spectroscopy. In F. Bergaya, B.K.G. Theng,

& G. Lagaly (Ed.), Handbook of Clay Science. (pp. 909–918). Elsevier.

Petit, S., Martin, F., Wiewiora, A., De Parseval, P., & Decarreau, A. (2004) Crystal-chemistry of talc: A near infrared (NIR) spectroscopy study. *American Mineralogist*, *89*, 319–326.

Russell, J.D. & Fraser, A.R. (1994) Infrared methods. In M.J. Wilson (Ed.), Clay Mineralogy: Spectroscopic and Chemical Determinative Methods (pp. 11–67). Dordrecht: Springer Netherlands.

Suquet, H., de la Calle, C., & Pezerat, H. (1975) Swelling and structural organization of saponite. *Clays and Clay Minerals*, *23*, 1–9.

Suquet, H., Iiyama, J.T., Kodama, H., & Pezerat, H. (1977) Synthesis and Swelling Properties of Saponites with Increasing Layer Charge. *Clays and Clay Minerals*, *25*, 231–242.

Trombetta, M., Busca, G., Lenarda, M., Storaro, L., Ganzerla, R., Piovesan, L., Lopez, A.J., Alcantara-Rodrìguez, M., & Rodríguez-Castellón, E. (2000) Solid acid catalysts from clays Evaluation of surface acidity of mono- and bi-pillared smectites by FT-IR spectroscopy measurements, NH3-TPD and catalytic tests. *Applied Catalysis A: General*, *193*, 55–69.

Trujillano, R., Vicente, M.A., Rives, V., Korili, S.A., Gil, A., Ciuffi, K.J., & Nassar, E.J. (2009) Preparation, alumina-pillaring and oxidation catalytic performances of synthetic Ni-saponite. *Microporous and Mesoporous Materials*, *117*, 309–316.

Trujillano, R., Rico, E., Vicente, M.A., Rives, V., Ciuffi, K.J., Cestari, A., Gil, A., & Korili, S.A. (2011) Rapid microwave-assisted synthesis of saponites and their use as oxidation catalysts. *Applied Clay Science*, *53*, 326–330.

Vicente, M.A., Suárez, M., López-González, J.D.D., & Bañares-Muñoz, M.A. (1996)

Characterization, surface area, and porosity analyses of the solids obtained by acid leaching of a saponite. *Langmuir*, *12*, 566–572.

Vogels, R.J.M.J., Kloprogge, J.T., & Geus, J.W. (2005) Catalytic activity of synthetic saponite clays: Effects of tetrahedral and octahedral composition. *Journal of Catalysis*, *231*, 443–452.

Walker, J.R. (1993) Chlorite polytype geothermometry. *Clays and Clay Minerals*, *41*, 260–267.

Xue, Z., Ma, J., Zheng, J., Zhang, T., Kang, Y., & Li, R. (2012) Hierarchical structure and catalytic properties of a microspherical zeolite with intracrystalline mesopores. *Acta Materialia*, *60*, 5712–5722.

Zhou, C.H., Zhou, Q., Wu, Q.Q., Petit, S., Jiang, X.C., Xia, S.T., Li, C.S., & Yu, W.H. (2019) Modification, hybridization and applications of saponite: An overview. *Applied Clay Science*, *168*, 136–154.